



**HAL**  
open science

## Importance of the double layer structure in the electrochemical deposition of Co from soluble $\text{Co}^{2+}$ - based precursors in Ionic Liquid media

Michal Tulodziecki, Jean-marie Tarascon, Pierre-Louis Taberna, Claude Guéry

### ► To cite this version:

Michal Tulodziecki, Jean-marie Tarascon, Pierre-Louis Taberna, Claude Guéry. Importance of the double layer structure in the electrochemical deposition of Co from soluble  $\text{Co}^{2+}$  - based precursors in Ionic Liquid media. *Electrochimica Acta*, 2014, 134, pp.55-66. 10.1016/j.electacta.2014.03.042 . hal-02019059

**HAL Id: hal-02019059**

**<https://hal.science/hal-02019059>**

Submitted on 14 Feb 2019

**HAL** is a multi-disciplinary open access archive for the deposit and dissemination of scientific research documents, whether they are published or not. The documents may come from teaching and research institutions in France or abroad, or from public or private research centers.

L'archive ouverte pluridisciplinaire **HAL**, est destinée au dépôt et à la diffusion de documents scientifiques de niveau recherche, publiés ou non, émanant des établissements d'enseignement et de recherche français ou étrangers, des laboratoires publics ou privés.



## Open Archive Toulouse Archive Ouverte (OATAO)

OATAO is an open access repository that collects the work of Toulouse researchers and makes it freely available over the web where possible

This is an author's version published in: <http://oatao.univ-toulouse.fr/21748>

**Official URL:** <https://doi.org/10.1016/j.electacta.2014.03.042>

**To cite this version:**

Tułodziecki, Michal and Tarascon, Jean-Marie and Taberna, Pierre-Louis<sup>✉</sup> and Guéry, Claude *Importance of the double layer structure in the electrochemical deposition of Co from soluble Co<sup>2+</sup> - based precursors in Ionic Liquid media.* (2014) *Electrochimica Acta*, 134. 55-66. ISSN 0013-4686

Any correspondence concerning this service should be sent to the repository administrator: [tech-oatao@listes-diff.inp-toulouse.fr](mailto:tech-oatao@listes-diff.inp-toulouse.fr)

# Importance of the double layer structure in the electrochemical deposition of Co from soluble $\text{Co}^{2+}$ - based precursors in Ionic Liquid media

M. Tułodziecki<sup>a</sup>, J.-M. Tarascon<sup>a</sup>, P.L. Taberna<sup>b</sup>, C. Guéry<sup>a,\*</sup>

<sup>a</sup> Laboratoire de Réactivité et Chimie des Solides and ALISTORE European Research Institute, UMR CNRS 7314, UFR des Sciences, 33 rue Saint Leu, 80039 Amiens cedex, France

<sup>b</sup> CIRIMAT/LCMIE and ALISTORE European Research Institute, UMR CNRS 5085, 31062 Toulouse cedex 9 - France

## ARTICLE INFO

### Key words:

Double Layer  
Ionic liquids  
Electrodeposition  
Cobalt  
EQCM  
Impedance Spectroscopy

## ABSTRACT

Electrodeposition in Ionic Liquid (IL) media is being widely used to obtain different metals, alloys and more recently binary compounds. However, the understanding of this process is still slim due to poor knowledge in the chemistry of ILs and also the complex structure of the double layer at the electrode surface. It is then difficult to predict deposition conditions when trying to synthesize a desired deposit. In this work, we provide insight into the processes taking place at the electrode by detailed studies of  $\text{Co}^{2+}$  reduction in ionic liquid media at elevated temperature, which have revealed an unusual Cyclic Voltammetry profile. A drastic drop in the reaction rate was observed, together with a well-shaped reduction peak during the oxidation sweep. Using Electrochemical Quartz Crystal Microbalance, Impedance Spectroscopy measurements and varying bath parameters, we ascribed those phenomena to the reconstruction of the double layer structure upon imposed polarization. Similar behaviors were observed for other systems ( $\text{Mn}^{2+}$ ,  $\text{Ni}^{2+}$ ,  $\text{Zn}^{2+}$ ). Finally, this work provides new insight into the electrochemical processes in ILs. We anticipate that it will also result in significant improvement in preparing metal and other deposits in the ionic liquid media.

## 1. Introduction

Ionic liquids (ILs) have received great attention in recent years as a media for electrodeposition thanks to their attractive chemical/physical properties. They are non-flammable, display very high thermal stability together with negligible vapor pressure, and are good solvents for numerous salts and polymers. Their wide window of electrochemical stability and relatively high conductivity have allowed the electrodeposition of less noble metals, semiconductors and alloys that could not be accomplished in aqueous solution due to its limited potential window and thermal stability[1–7]. More recently binary compounds such as sulfides[8,9] and metal oxides[10–12] have been electrodeposited from IL baths, opening new possibilities for this media.

An issue of primary importance regarding electrodeposition processes is the structure of the double layer and its behavior under applied potential which is different in ILs, aqueous solution and

other molecular solvents. It has been proven both theoretically and experimentally that the cations and anions of ILs are highly structured, forming layers within the double layer [1,13–16]. Depending on surface polarization, the arrangement and conformation of the anions and cations may change as proven by Atomic Force Microscopy[17] and Sum Frequency Generation Spectroscopy[18].

Cobalt and its alloys are very important functional materials due to their magnetic properties, and resistance to corrosion, temperature and wear. Electrodeposition of Co is relatively difficult from aqueous solutions due to hydrogen evolution[19,20], necessitating to shift to more stable solvents such as ionic liquids. Katayama's[21,22] and Guo's[23] studies have shown that  $\text{Co}^{2+}$  undergoes  $2e^-$  reduction with high overpotential. Slow kinetics of the reduction process was ascribed to the existence of a huge octahedral cobalt complex  $[\text{Co}(\text{TFSI})_3]^-$ . Katayama et al. have further shown that the reduction overpotential decreases with temperature, and they attribute this effect to the dissociation of the  $[\text{Co}(\text{TFSI})_3]^-$  complex, based on the change of bath color from pink (octahedral complexation) to blue (tetrahedral complexation) at high temperature[21]. The tetrahedral cobalt complex was also obtained by either changing a cobalt salt ( $\text{CoCl}_2$  in BMPTFSI)[24] or

\* Corresponding author.

E-mail address: [claude.guery@u-picardie.fr](mailto:claude.guery@u-picardie.fr) (C. Guéry).

by adding strong organic complexing agents as TU[22,25]. Despite all these researches, issues dealing with double layer structuring and cation complexation, which are of crucial importance for understanding and planning electrochemical processes in IL media, are still not well known, hence our motivation to address them.

In this study, we perform a detailed investigation of the  $\text{Co}^{2+}/\text{Co}$  electrochemical reduction process in ionic liquid media by exploring the influence of temperature, substrate, nature of the ionic liquid (with focus on EMImTFSI), and complexation of  $\text{Co}^{2+}$ . Special attention is devoted to the fundamental aspects of the processes taking place at the electrode surface via the complementary use of Electrochemical Quartz Crystal Microbalance (EQCM), Cyclic Voltammetry (CV) and Impedance Spectroscopy (IS) measurements. Some interesting phenomena, never reported previously for the  $\text{Co}^{2+}/\text{Co}$  system, have been unravelled. Finally we attempt to explain them based on our results and the large amount of literature data on ionic liquids.

## 2. Experimental

The electrochemical bath was composed of  $\text{Co}(\text{TFSI})_2$  (Solvionic) solution in IL either EMImTFSI, OMImTFSI, BMPTFSI, BMImTfO or tBMNTFSI ordered from Solvionic, 99.9% pure ( $\text{H}_2\text{O} < 0.005\%$ ), Table 1. Prior to being used, the ILs were purified under vacuum at  $75^\circ\text{C}$  for 2 days; the final water content was  $\sim 6$  ppm as checked by Karl Fischer measurement. The complexing agent Thiourea (from Aldrich) was used as received. The  $\text{Co}(\text{TFSI})_2$  salt was chosen as cobalt cation precursor in order to avoid the addition of highly corrosive chlorides ( $\text{CoCl}_2$ ). If not otherwise specified, the initial concentration of cobalt cations was 0.12 M. All the substances were kept in an argon-filled glove box ( $\text{O}_2$  and  $\text{H}_2\text{O} < 0.1$  ppm). In all TFSI<sup>-</sup> based ILs (containing only  $\text{Co}^{2+}$  cations) the color of the bath was purple indicating octahedral coordination of cobalt cations  $[\text{Co}(\text{TFSI})_3]^-$ . We have just noted a minor change of the bath color (0.12 M  $\text{Co}(\text{TFSI})_2$  in EMImTFSI) from purple (RT) to dark purple upon heating (up to  $200^\circ\text{C}$ ), suggesting only a slight temperature influence on the cobalt coordination. This contrasts with the results presented by Katayama et al. where the solution of  $\text{Co}(\text{TFSI})_2$  in BMPTFSI changed to blue at high temperature[21]. However Raman/IR results have recently revealed the absence of change in coordination number as a function of temperature, although the conformational equilibrium in the coordination sphere (between two most stable states cis and trans) has been found to be strongly dependent[26].

A three-electrode set-up was used for electrochemical measurements (chronoamperometry, cyclic voltammetry, impedance spectroscopy). Five different substrates were used as working electrodes (WE): platinum disc (Ptd)  $S = 1.78 \text{ cm}^2$ , platinum planar electrode (Ptp)  $S = 0.020 \text{ cm}^2$ , glassy carbon planar electrode (GC)  $S = 0.071 \text{ cm}^2$ , platinum and stainless steel wires (Ptw and SSw respectively). The surface area of the last one was estimated according to the length of the dipped part (surface ranging from 0,017 to 0,033  $\text{cm}^2$ ). The counter electrodes (CE) were platinum grids with high surface area ( $S \approx 2 \text{ cm}^2$  and  $10 \text{ cm}^2$  depending on the chosen WE). An Ag wire covered with  $\text{Ag}_2\text{O}$  was used as the pseudo reference electrode (RE). The stability of RE at high temperature has been checked by means of OCP stability and reproducibility. It was found stable enough for the purpose of our experiments. All the values of potential will be given versus the pseudo  $\text{Ag}/\text{Ag}_2\text{O}$  reference electrode if not otherwise specified. Prior to being used, the platinum WEs were annealed in 0.5 M  $\text{H}_2\text{SO}_4$  in order to obtain a stress-free and clean surface (the CV profile patterns were comparable with now standard ones representative of an impurity free Pt surface)[27]. Next, the electrodes were rinsed with distilled water, ethanol, acetone and deionized water. The CE electrode was cleaned

in 0.5 M nitric acid in an ultrasonic bath for 1 h, and then intensively rinsed with distilled water, ethanol, acetone and deionized water. All the components of the cell were dried in an oven at  $T = 50^\circ\text{C}$  for 2 hours before the experiment. Preparation of the solution and assembly of the cell were done in a glove box. The cell was immersed in an oil bath while the temperature was controlled with  $\pm 2^\circ\text{C}$  difference between heating and deposition bath.

The electrochemical measurements were carried out with an Autolab PGSTAT 30 potentiostat (Eco Chemie BV). The impedance measurements were conducted with a Biologic VSP potentiostat; collection of impedance data started after the system reached steady state conditions at fixed potential. The chosen frequency ranged from 1 MHz to 50mHz while the amplitude of sinusoidal potential was set to 10 mV. All the CV measurements were performed starting from the OCP with a reduction scan followed by the oxidation one if not otherwise specified.

The obtained deposits on Ptd were soaked in chloroform to remove adsorbed IL from the surface. Their morphology was further analyzed using a Philips XL 30 field emission gun FEG microscope.

EQCM measurements were carried out using a commercial SEIKO microbalance with AT-cut 9 MHz quartz covered with platinum on both sides. The electro-active geometric surface area was equal to  $S = 0.196 \text{ cm}^2$ . Simultaneous measurements of the quartz frequency and motional resistance were done in order to follow both the change in mass and the variation in  $\text{Co}^{2+}$  concentration in the vicinity of the electrode (by following the change of viscosity and density product of the solution)[12,28,29]. The EQCM was calibrated with CV measurement in 0.05 M solution of  $\text{AgTFSI}$  in EMImTFSI, at  $100^\circ\text{C}$ , with  $2 \text{ mV}\cdot\text{s}^{-1}$  scanning rate. The proportionality constant ( $\Delta m = C \cdot \Delta f$ ) was determined between the change of quartz frequency ( $\Delta f$ ) and change of deposited mass ( $\Delta m$ )[30]. A constant value  $C = 1.065 \cdot 10^{-9} \text{ g}\cdot\text{Hz}^{-1}$  close to the theoretical one  $C_t = 1.068 \cdot 10^{-9} \text{ g}\cdot\text{Hz}^{-1}$  was found, suggesting that issues regarding viscosity of the bath or roughness of the substrate can be neglected. So, to analyze the EQCM data, the function  $M/z$  (molar mass over number of exchanged electrons) was simply calculated according to Sauerbrey equation (1) and Faraday's laws of electrolysis (2), assuming that the reaction efficiency is near 100% (3). The  $M/z$  value was calculated from the  $\Delta f$  and  $\Delta Q$  difference between each adjacent point.

$$\Delta m = -C\Delta f \quad (1)$$

$$\Delta m = \left(\frac{\Delta Q}{F}\right) \left(\frac{M}{z}\right) \quad (2)$$

$$\frac{M}{z} = - (FC) \frac{\Delta f}{\Delta Q} \quad (3)$$

The expected value of  $M/z$  for the growth of Co, which relies on a  $2 e^-$  process, is  $29.5 \text{ g}\cdot\text{mol}^{-1}$ . The CV with scanning rate  $2 \text{ mV}\cdot\text{s}^{-1}$  and probe time 1 s, was performed in 0.12 M  $\text{Co}(\text{TFSI})_2$  solution in EMImTFSI at  $100^\circ\text{C}$  under Ar atmosphere.

All the experiments were done several times to check the repeatability. We would also like to mention that  $\text{Co}^{2+}/\text{Co}^+$  symbols are mostly written as cobalt species in the solution instead of complexated forms, which they are in reality ( $[\text{Co}(\text{TFSI})_3]^- / [\text{Co}(\text{TFSI})_x]^{y-}$ ), although we come back to the latter when it is needed for the sake of clarity.

## 3. Results

### 3.1. Cyclic Voltammetry in EMImTFSI

We initially checked the electrochemical response of 0.12 M  $\text{Co}^{2+}$  solution in EMImTFSI IL, at  $100^\circ\text{C}$ , on 3 different substrates: Ptp, GC and SSw (Fig. 1a, b, c respectively). Whatever the nature of the substrate, CVs revealed identical features during the

**Table 1**  
Abbreviations for the IL components and their structures.

IL component full name	Abbreviation	Structure
1-ethyl-3-methylimidazolium cation	EMIm <sup>+</sup>	
1-butyl-3-methylimidazolium cation	BMIm <sup>+</sup>	
1-octyl-3-methylimidazolium cation	OMIm <sup>+</sup>	
tri-butyl-methylammonium cation	tBMN <sup>+</sup>	
1-butyl-1-Methylpyrrolidinium cation	BMP <sup>+</sup>	
bis(trifluoromethylsulfonyl)imide anion	TFSI <sup>-</sup>	
trifluoromethanesulfonate anion	TfO <sup>-</sup>	
dicyanamide anion	DCA <sup>-</sup>	

reduction and oxidation sweeps (Fig. 1 I, II, III, IV, V, insets). Following the reduction sweep on the Ptp electrode (Fig. 1a, black curve), the first reduction peak with an onset at  $-0.70\text{V}$  and centered at  $-0.88\text{V}$  (I) is ascribed to  $\text{Co}^{2+}$  reduction. The reduction starts at a high overpotential of  $\sim 0.8\text{V}$  as compared to the coupled oxidation process (onset  $\sim 0\text{V}$ ). Subsequently, between  $-0.9\text{V}$  and  $-1.1\text{V}$  a diffusion limited process appears as the current density tends to stabilize. At lower potentials, the reduction current density suddenly drops and reaches a minimum at  $-1.20\text{V}$  (II). Afterwards, the reduction current density increases again and reaches the maximum at  $-1.38\text{V}$  (III), which we again assigned to the reduction of  $\text{Co}^{2+}$ . The value of the limiting current density below  $-1.38\text{V}$  is similar to the one of diffusion limited reaction taking place between  $-0.9$  and  $-1.1\text{V}$ . On the reverse sweep (Fig. 1a, red curve), the current density progressively decreases and reaches a minimum at slightly higher potentials ( $-1.18\text{V}$ ) in comparison to the reduction sweep ( $-1.20\text{V}$ ). Above  $-1.18\text{V}$ , a very sharp reduction peak centered at  $-1.09\text{V}$  is observed (IV), followed by a diffusion limited and then a diffusion/activation limited reduction process. The oxidation signal at more positive potentials was ascribed to Co stripping. The reversibility (the charge ratio between oxidation and reduction process) of the electrochemical reaction is above 75%; however, it varies according to the chosen reverse potential reaching almost 100% at higher potentials (Supplementary Materials (SM), Fig. 1\*). Such aforementioned features, namely the drop in current density around  $-1.2\text{V}$  and the oxidation peak on the reverse sweep, were

also observed for the other substrates with slight shifts in onset and peak potentials (Fig. 1b, c).

### 3.2. EQCM measurement

Both the huge drop in current during the reduction sweep and the well-defined reduction peak during the oxidation sweep are rare phenomena in electrochemistry. To gain further insight into the origins of these unusual features, we have conducted an EQCM measurement which is an elegant technique to indirectly determine the mass of the deposit as well as the concentration of  $\text{Co}^{2+}$  near the electrode via quartz frequency and motional resistance changes, respectively. Cyclic voltammetry at a rate of  $2\text{mV}\cdot\text{s}^{-1}$ , at  $100^\circ\text{C}$ , in  $0.12\text{M Co}(\text{TFSI})_2$  was performed. The reverse potential was chosen at the minimum of the current drop during the reduction sweep ( $-1.20\text{V}$ ).

Figs 2a, b, c, d show current, quartz frequency, quartz resistance and  $M/z$  variations versus potential, respectively. The current profile is almost identical to the one obtained on the Ptp electrode in the same conditions (Fig. 1a). A shift in potential is visible most likely due to minor differences in the Pt surface, which in case of quartz is electrochemically mirror polished as opposed to mechanically. Whatever the origin of the shift, a drop in current density with the minimum at  $-1.20\text{V}$  and a very sharp reduction peak during the oxidation sweep are still observed. The reduction of  $\text{Co}^{2+}$  species starts at slightly lower potentials of  $-0.87\text{V}$  and is centered

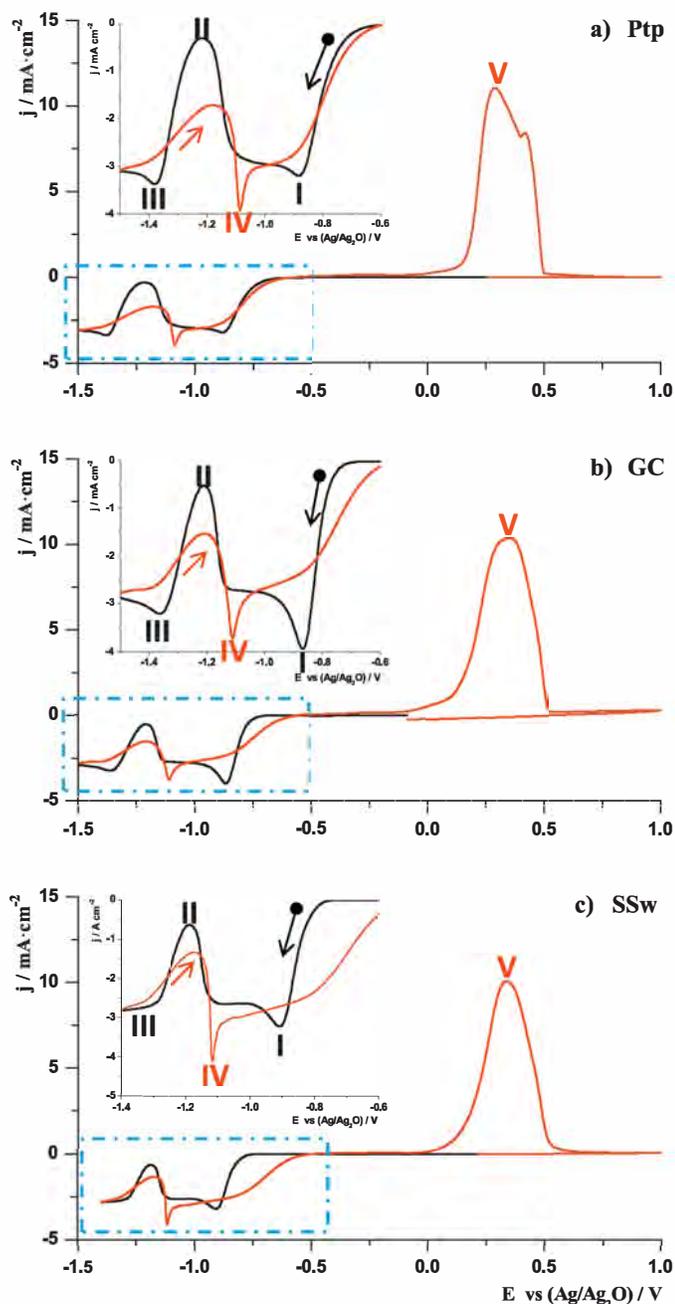


**Fig. 1.** CV's curves of 0.12 M Co(TFSI)<sub>2</sub> solution in EMImTFSI at 100 °C, on: a) Ptp, b) GC, c) SSw electrode. The black curve presents the reduction sweep while the red oxidation sweep. CE–Pt, RE–Ag/Ag<sub>2</sub>O, scanning rate 5 mV·s<sup>-1</sup>. Inset: magnification of negative potential part.

at -0.96 V. A time derivative of the current (SM, Fig. 2a\*) reveals two weak anomalies at -0.88 and -0.92 V. Further, comparing CV (Fig. 2a) and variation in quartz frequency (Fig. 2b) between -0.87 and -0.90 V (within the blue dashed lines potential window, Fig. 2), a high reduction current density is observed while only small changes in frequency occurred (clearly visible on the time derivative of the frequency which is proportional to the current according to Sauerby and Faradays equations - SM, Fig. 2b\*). Additionally, a small decrease in motional resistance (Fig. 2c) is observed, attributed to the change of viscosity/density properties of the solution in the vicinity of the electrode. In our opinion, this part of the reduction process involves only soluble species with 1e<sup>-</sup> reduction process of Co<sup>2+</sup> (equation 4), and the aforementioned variation in motional

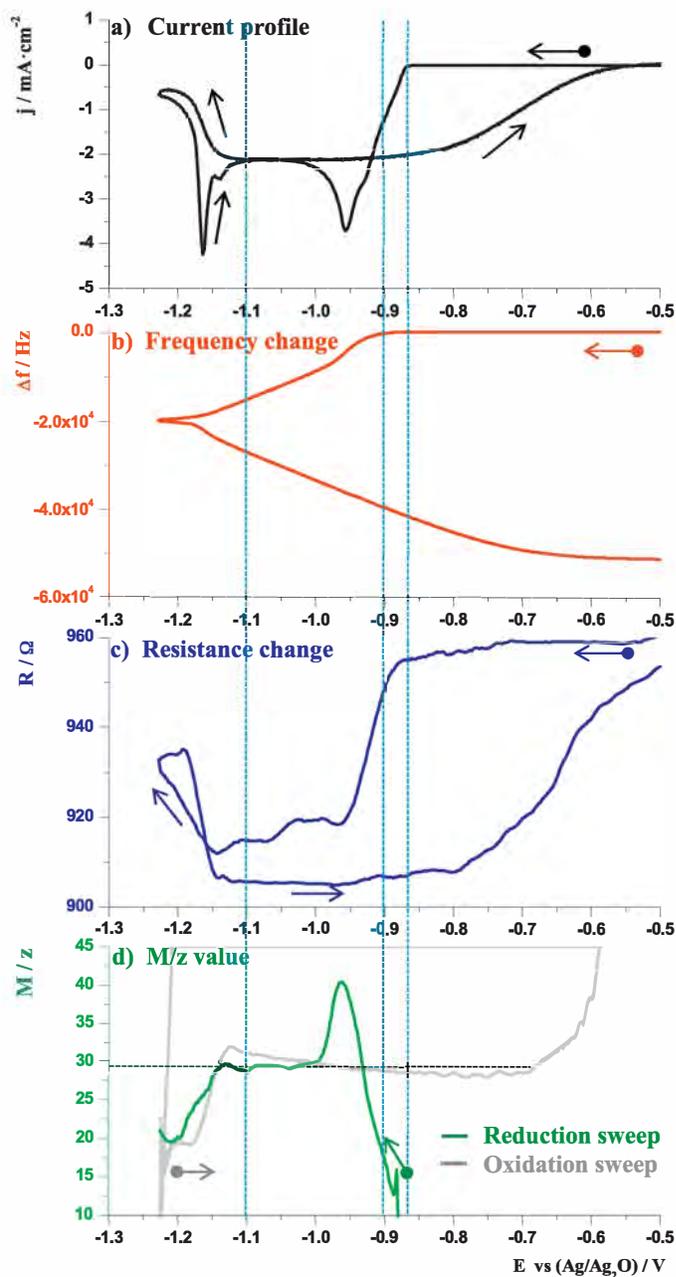


**Fig. 2.** EQCM measurement a) current versus potential, b) quartz frequency change versus potential, c) quartz motional resistance versus potential, d) calculated M/z value for the reduction sweep–green curve and oxidation sweep–gray curve, the black dashed line indicates the theoretical M/z value of Co formation. Blue dashed lines divide the CV curve into regions where different phenomena occur. 0.12 M Co(TFSI)<sub>2</sub>, T = 100 °C, WE–Pt mirror polished on quartz, CE–Pt, RE– Ag/Ag<sub>2</sub>O, scan rate 2 mV·s<sup>-1</sup>.

resistance is due to the change in the coordination sphere of Co<sup>2+</sup> as it is reduced.



Below -0.9 V, there is a significant decrease in frequency that is accompanied by the appearance of a dark deposit on the quartz, indicating the consumption of Co<sup>2+</sup>/Co<sup>+</sup> cations according to equations (5) and (6). This leads to a decrease of solution viscosity/density, in agreement with the quartz motional

change (Fig. 2c) that suddenly starts to decrease and then stabilize at  $R=915\ \Omega$  in the region of the diffusion limiting step (-1.0/-1.1 V). Calculated  $M/z$  values (Fig. 2d) start to progressively increase reaching a maximum of  $42\ \text{g}\cdot\text{mol}^{-1}$  at  $E=-0.97\ \text{V}$ . This maximum most likely originates from the simultaneous reduction of  $\text{Co}^{2+}$  and  $\text{Co}^+$  species which should theoretically give  $M/z$  values of  $29.5\ \text{g}\cdot\text{mol}^{-1}$  and  $59\ \text{g}\cdot\text{mol}^{-1}$ , respectively. Afterwards,  $M/z$  stabilizes at a value of  $29\text{--}30\ \text{g}\cdot\text{mol}^{-1}$  indicating a direct 2 electron  $\text{Co}^{2+}$  reduction process at lower potentials (equation 6). Once the current density starts to drop (below -1.1 V, blue dashed line Fig. 2), the frequency tends to stabilize due to a slowdown in the deposition rate; more importantly, the motional resistance increases dramatically (increase in viscosity and density product) reaching  $935\ \Omega$ . This is in relation with the diffusion of the  $\text{Co}^{2+}$  in the vicinity of the electrode, equalizing its concentration with the bulk one.

When the potential is reversed, a huge and very sharp reduction peak is observed. It is linked to both a sudden increase in the deposition rate and a decrease in motional resistance (drop in viscosity and density product). This means that  $\text{Co}^{2+}$  reduction resumes rapidly with therefore the onset of a diffusion limiting process (as further suggested by the constancy of the motional resistance) at the plateau of the motional resistance value ( $R=905\ \Omega$ ). Overall, from the current profile, quartz frequency and quartz motional resistance variation, it seems that the reduction of  $\text{Co}^{2+}$  around -1.2 V is inhibited by a reversible potential triggered phenomenon.

At this stage, it should be recalled that the quartz motional resistance does not solely depend on the bath viscosity and density product; other parameters such as viscoelasticity, roughness or adhesion of the deposit also contribute to the motional resistance [29,31]. However, in our case, the shape of the motional resistance curve follows the change in current density which is proportional to the change of  $\text{Co}^{2+}$  concentration. The change in  $\text{Co}^{2+}$  content affects the structure of IL in the vicinity of the electrode (diffuse layer of  $\text{Co}^{2+}$ ) that acts as a viscoelastic film on the quartz electrode. Any variation in IL structure leads to changes in the viscosity/density parameter consequently affecting the motional resistance. Additionally, note that during the diffusion limited reduction process (-1.1 V to -0.8 V on oxidation sweep and -1.0 to -1.1 V on reduction sweep), the motional resistance remains almost constant ( $R \approx 905\ \Omega$ ). Moreover its value is close to the quartz resistance in pure IL solution at  $100^\circ\ \text{C}$  ( $R=895\ \Omega$ ), while there is still a progressive evolution of the deposit. This led us to conclude that the growth of the Co deposit has negligible impact on the resistance which mostly depends on the properties of the diffuse layer (viscosity/density) that is related to  $\text{Co}^{2+}$  concentration.

### 3.3. Influence of the bath parameters

In order to further investigate the origin of the sudden drop in current density during reduction at -1.20 V (Fig. 1), the influence of temperature, IL formulation, and complexation of  $\text{Co}^{2+}$  cations on the CV response were checked. All the experiments were conducted on the PtW electrode if not otherwise specified. The CV curve collected at  $100^\circ\ \text{C}$  in  $0.12\ \text{M}\ \text{Co}(\text{TFSI})_2$  in EMImTFSI (Fig. 3a) is a blank test that will be treated as a reference through the rest of this paper.

#### 3.3.1. Temperature

Fig. 3 represents CV curves of  $0.12\ \text{M}\ \text{Co}(\text{TFSI})_2$  solutions at different temperatures. At RT (Fig. 3b, black curve), a single peak (I) with huge overpotential ( $\sim 1.5\ \text{V}$ ) is observed as opposed to two at  $100^\circ\ \text{C}$ . However during the next cycle (Fig. 3b, red curve) an additional reduction peak (II) appears at slightly higher potentials (onset at -1 V). The intensity of the reduction peak (II) progressively increases with the number of cycles while the intensity of the reduction peak (I) decreases (Fig. 3b, inset); this suggests that in both reactions the same species, namely the  $\text{Co}^{2+}$  cations, are

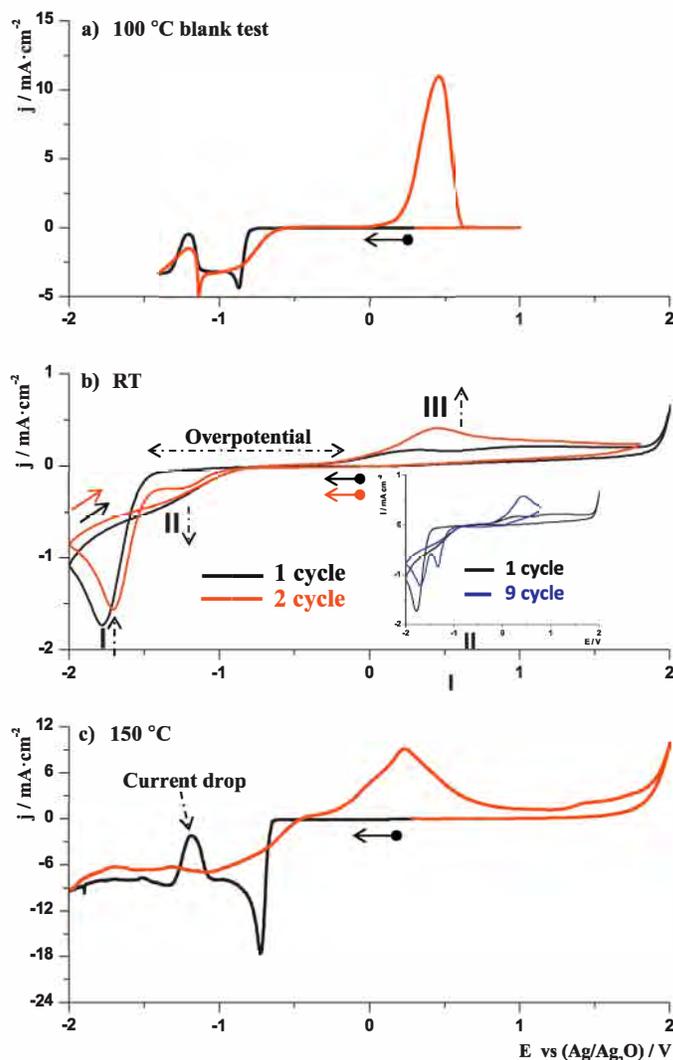


Fig. 3. CV's curves of  $0.12\ \text{M}\ \text{Co}(\text{TFSI})_2$  solution in EMImTFSI at different temperatures a) blank test at  $100^\circ\ \text{C}$  b) 2 successive scans at RT, inset represents first and ninth cycle, c)  $150^\circ\ \text{C}$ . WE-Ptw, CE-Pt, RE-Ag/Ag<sub>2</sub>O, scanning rate  $5\ \text{mV}\cdot\text{s}^{-1}$ .

reduced. The reduction/oxidation process at RT is poorly reversible (33%) as on the reverse sweep, only a small oxidation peak (III) is visible during the first cycle (Fig. 3b, black curve). The reversibility improves upon cycling, due to the appearance of a new reduction peak (II) that is almost 100% reversible (SM, Fig. 3\*). On the other hand, at high temperature ( $T=150^\circ\ \text{C}$ , Fig. 3c), the same phenomena (onset of 2 reduction peaks together with a sudden drop in the current density) are observed alike at  $100^\circ\ \text{C}$ . The minimum of the current density drop is slightly shifted to higher potentials (-1.18 V).

#### 3.3.2. IL nature

One of the advantages of ILs is the possibility of playing with their formulation by substituting either their cation or anion, and hence changing greatly their physical and chemical properties and their interactions with cobalt cations and the substrate.

First, substitution of  $\text{TFSI}^-$  with  $\text{TfO}^-$  was investigated. Once the  $\text{Co}(\text{TFSI})_2$  is added to the  $\text{TfO}^-$  based IL, its color changes to blue meaning that the coordination is no longer octahedral ( $[\text{Co}(\text{TFSI})_3]^-$ ) as in the case of EMImTFSI, but tetrahedral ( $[\text{Co}(\text{TfO})_4]^{2-}$ ) as deduced from the collected UV-VIS spectra (SM, Fig. 4\*). Fig. 4a shows the CV curve of  $0.12\ \text{M}\ \text{Co}(\text{TFSI})_2$  solution in EMImTfO IL at  $100^\circ\ \text{C}$ . Although the shape of the peaks as well as their onsets change significantly (the reduction of  $\text{Co}^{2+}$  starts at

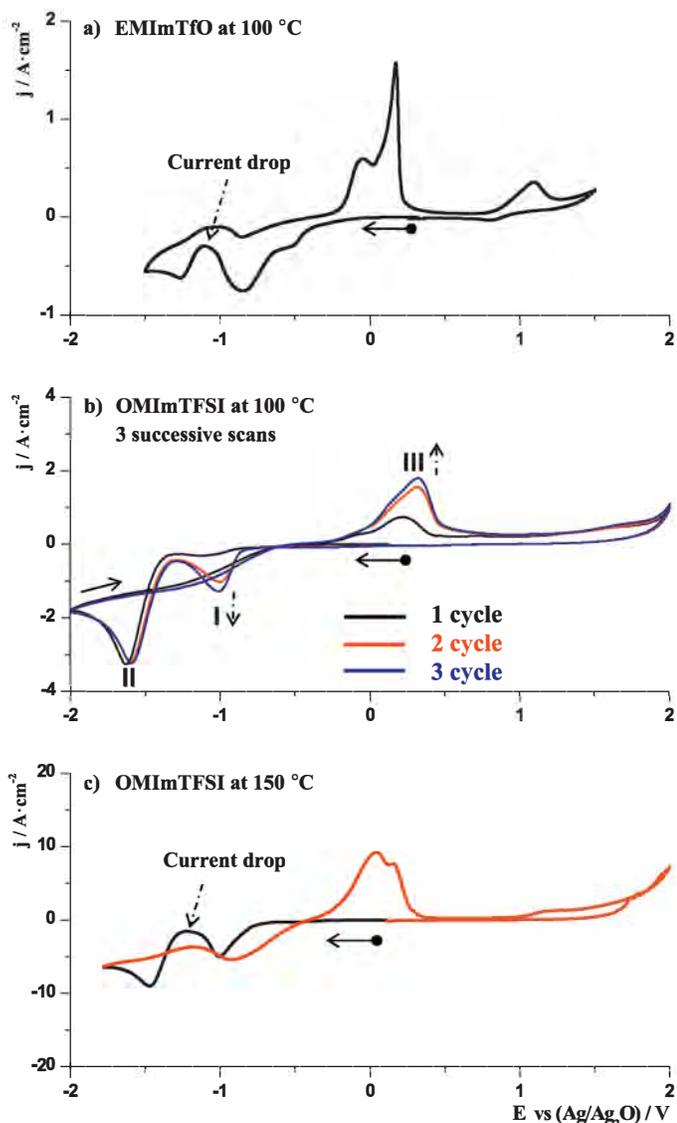


**Fig. 4.** CV of 0.12 M  $\text{Co}(\text{TFSI})_2$  solution: a) in EMImTfO at 100 °C, b) in OMImTFSI at 100 °C 3 successive scans, c) in OMImTFSI at 150 °C. WE–Ptw, CE–Pt, RE–Ag/Ag<sub>2</sub>O, scanning rate 5 mV·s<sup>-1</sup>.

higher potentials), the two reduction peaks separated by a drop in current density are still visible, as well as the reduction peak on the oxidation sweep (SM, Fig. 5\*).

The influence of imidazolium ring back bone was checked by substituting the EMIm<sup>+</sup> cation with OMIm<sup>+</sup>. The successive CV curves of 0.12 M  $\text{Co}(\text{TFSI})_2$  on the Ptw at 100 °C in OMImTFSI IL are reported on Fig. 4b. On the first scan (black curve), a small reduction peak (I) starting at -0.89 V and centered at -1.12 V followed by a huge reduction peak (II) with the onset at -1.30 V and centered at -1.62 V are observed; both features were assigned to the reduction of  $\text{Co}^{2+}$ . In the next scans, the intensity of both the reduction peak (I) and the oxidation peak (III) increase. That is very similar to the CVs obtained in 0.12 M  $\text{Co}(\text{TFSI})_2$  in EMImTFSI at RT (Fig. 3b); nevertheless, in the case of OMImTFSI at 100 °C the intensity of the peak at -1.60 V (II) does not change upon cycling. At higher temperature (150 °C), the intensity of the first peak is greatly enhanced in comparison to the second one (Fig. 4c). Additionally, a very clear drop in current density is visible, reaching again the minimum at -1.20 V. Similarly, a reduction peak on the oxidation sweep is observed as well (more clear when the potential is reversed at -1.20 V, (SM, Fig. 6\*).

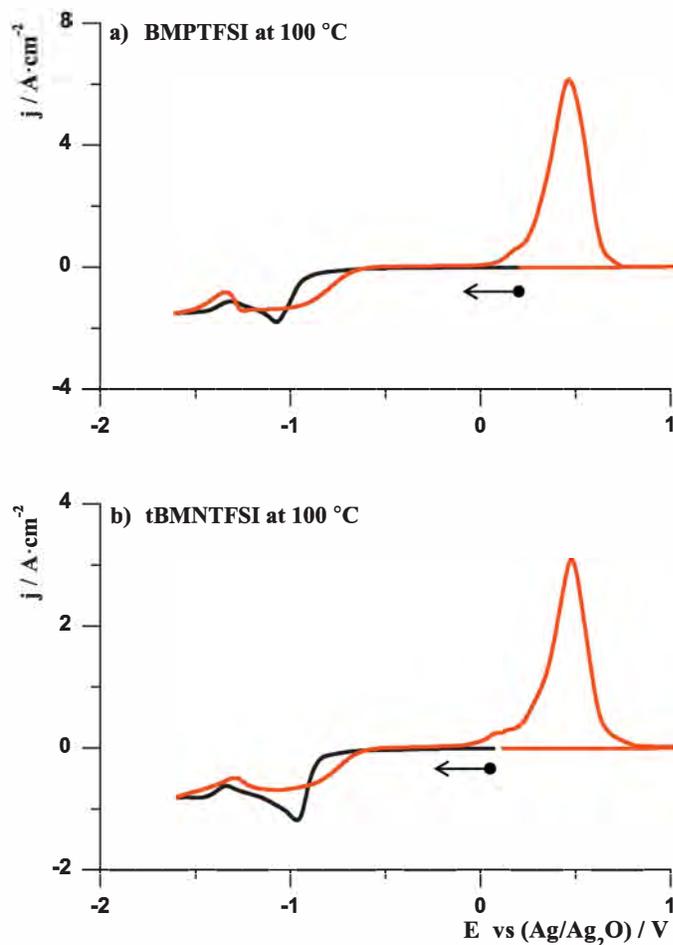


**Fig. 5.** CV of 0.12 M  $\text{Co}(\text{TFSI})_2$  solution in a) BMPTFSI at 100 °C and b) tBMNTFSI at 100 °C. WE–Ptw, CE–Pt, RE–Ag/Ag<sub>2</sub>O, scanning rate 5 mV·s<sup>-1</sup>.

Lastly, the IL cation was replaced by BMP<sup>+</sup> and tBMN<sup>+</sup>. In both cases, two reduction peaks are visible (Fig. 5a and b, respectively); however, the drop in current density is not so significant as for the imidazolium based ILs described above (the density current at the minimum of the drop is very high as compared to blank test, Fig. 3a),

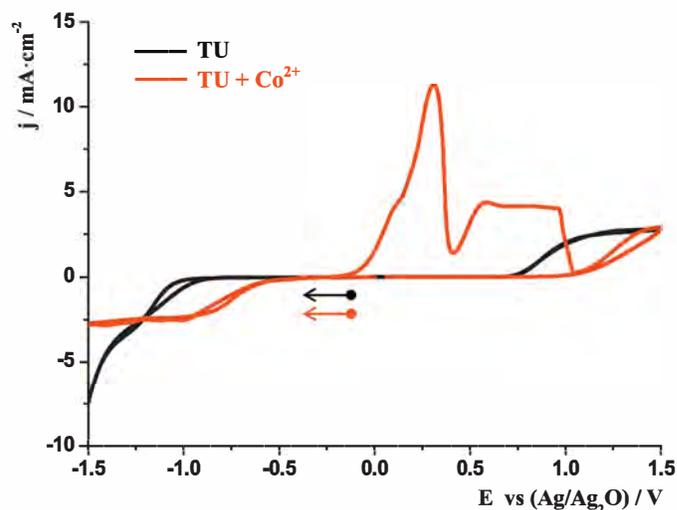


**Fig. 6.** CV curves of EMImTFSI solution containing 0.48 M TU – black curve and 0.12 M  $\text{Co}(\text{TFSI})_2$  – red curve, at 100 °C on Ptp electrode. CE–Pt, RE–Ag/Ag<sub>2</sub>O, scanning rate 5 mV·s<sup>-1</sup>.



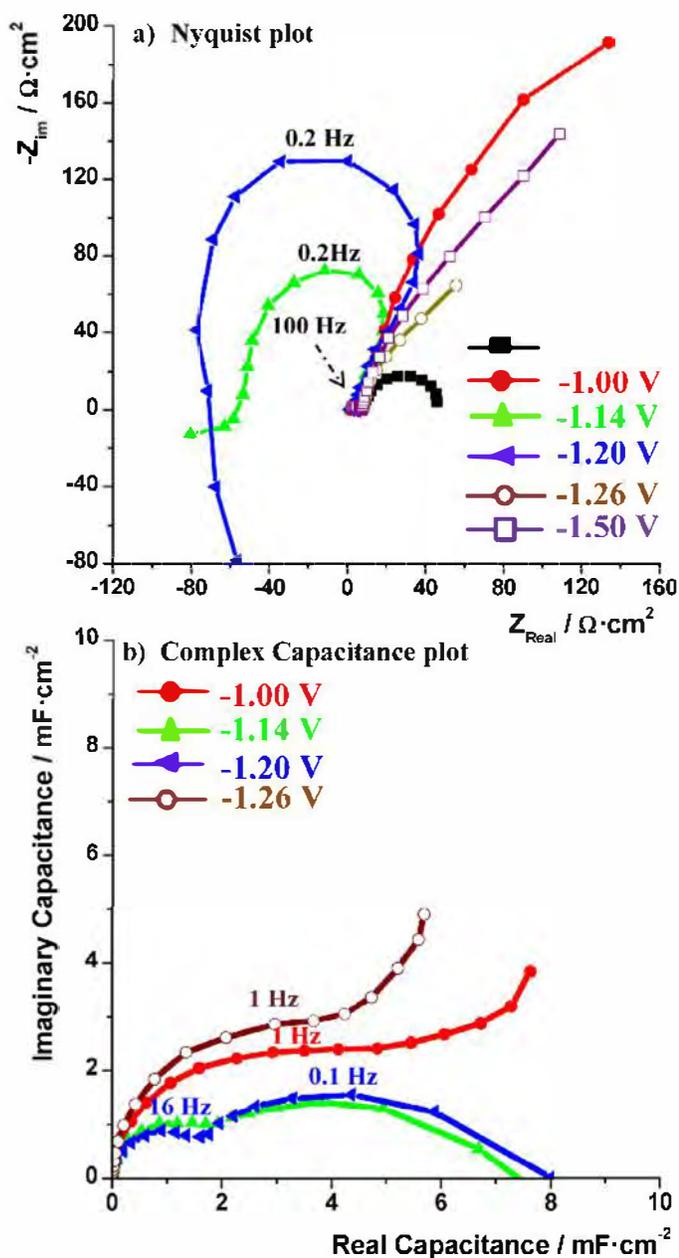


**Fig. 7.** Impedance spectroscopy of 0.12 M Co(TFSI)<sub>2</sub> solution at 100°C at different potentials a) Nyquist plots: -0.8V black filled squares, -1.00V red filled circles, -1.14V green filled triangles, -1.20V blue filled tilted triangles, -1.26V brown open circles, -1.50V purple open squares. b) Complex capacitance curves: -1.00V red filled circles, -1.14V green filled triangles, -1.20V blue filled tilted triangles, -1.26V brown open circles. The inset represents zoom of the curves at very high frequencies. WE-Ptp, CE-Pt, RE- Ag/Ag<sub>2</sub>O.

even at high temperatures (SM, Fig. 7\*). Additionally, the minimum of the current density drop is shifted to lower potentials, -1.34 V for BMP<sup>+</sup> and -1.35 V for tBMN<sup>+</sup>.

So overall, it turns out that the nature of the cation solely influences both the current drop during reduction and the reduction peak on the reverse sweep.

### 3.3.3. Complex charge

As a last part of our survey, the influence of the charge of the cobalt complex was investigated, which is negatively charged in either TFSI<sup>-</sup> or TfO<sup>-</sup> based IL. To assess such a parameter, a neutral complexing agent thiourea (known to produce positive [Co(TU)<sub>4</sub>]<sup>2+</sup> complexes) was added to a 0.12 M Co(TFSI)<sub>2</sub> solution in EMImTFSI

IL[22]. Upon addition of TU, the solution rapidly turns blue, meaning that the complexation changed from octahedral [Co(TFSI)<sub>3</sub>]<sup>-</sup> to tetrahedral [Co(TU)<sub>4</sub>]<sup>2+</sup>. Fig. 6 displays the CV curves on the Ptp electrode of EMImTFSI solution containing 0.48 M TU (black curve) and 0.48 TU + 0.12 M Co(TFSI)<sub>2</sub> (red curve). The same Ptp electrode with constant surface area was used in both cases to directly compare the intensities. The stability window for the TU, which ranges from -1.0 to 0.8V, can be widened upon the addition of metal cations. Lastly, the onset of TU oxidation shifts to 1 V (SM, Fig. 8\*) while its reduction is highly hindered (Fig. 6). Indeed since the current profile indicates steady state diffusion (Co<sup>2+</sup> reduction) while the solution with only TU reveals a continuous increase in current density. Reduction of the Co<sup>2+</sup> starts at relatively high potential E = -0.5 V and is followed by a single reduction wave without any current drop and reduction peak on the reverse scan, unlike previously described systems. Following the oxidation sweep, an additional oxidation wave is observed starting at 0.41 V (apart from Co stripping process at 0.3 V), however, for the sake of conciseness, it will not be discussed further. We can thus conclude from the aforementioned results that the charge of the complex is also one of the crucial parameters responsible for the unusual behavior observed during the reduction/oxidation sweeps.

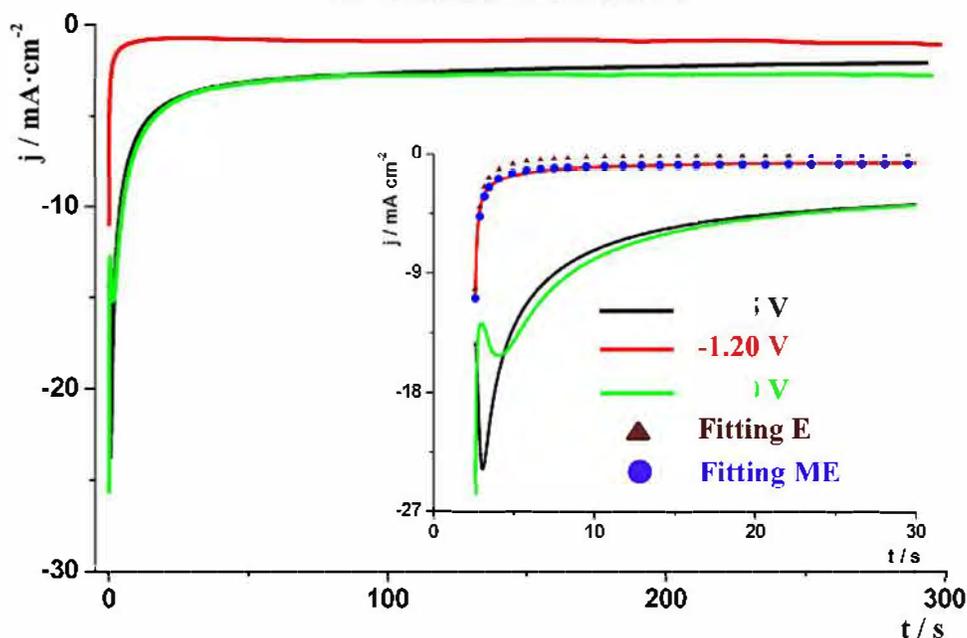
### 3.4. Impedance spectroscopy: Nyquist and Cole-Cole plots

The dynamic aspect of the system was tested by potentiostatic electrochemical impedance spectroscopy at different potentials (-0.80; -1.00; -1.16; -1.20; -1.26; -1.50V). For each experiment, a newly prepared electrode was used. All the impedance spectra were collected after the steady state was reached at each applied potential. Fig. 7a reports the Nyquist impedance curves of 0.12 M Co(TFSI)<sub>2</sub> solution at 100°C on the Ptp electrode. At -0.80V (full black squares), a semicircle (42 Ω·cm<sup>2</sup> of diameter) is observed and can be assigned to parallel association of the charge transfer resistance and the double layer capacitance. As the potential decreases (-1.00V), a sharp increase of the imaginary part, probably related to diffusion limitation, is noticed. At -1.14V (green full triangles) and -1.20V (blue full triangles) for lower frequencies, a second semicircle appears with the opposite sign of curvature, crossing the negative part of the real axis at finite frequencies (negative impedance). This is in agreement with our CV curve, where in between -1.1 and -1.2V a negative slope on the voltammogram is observed (Fig. 1a) leading to negative value of polarization resistance. The negative impedance further disappears at lower potentials (-1.26 and -1.50 V, brown empty circle and purple empty square, respectively) at the expense of a half semicircle (however a Warburg impedance cannot be excluded).

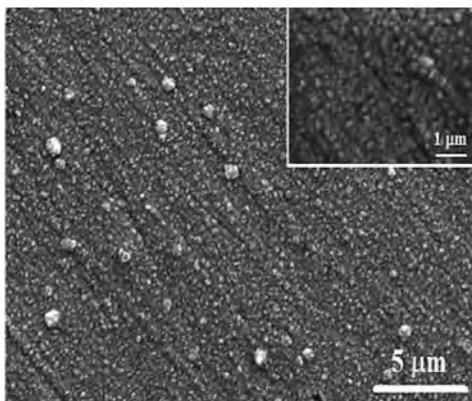
The above mentioned negative impedance is a part of wider consideration on the stability nature of the system. If the intersection of the impedance spectra happened in the origin of the complex impedance plane, a Hopf-bifurcation (since the crossing happens at finite frequencies) would appear leading to an oscillatory current profile at fixed potential[32]. The shift of the intersection can be done by either applying a sufficient external resistance or changing the deposition parameters. To our surprise, a very clear oscillation current could be obtained at fixed potential of -1.16V without any additional resistance (SM, Fig. 9\*). In our opinion, the freshly deposited Co can act as the additional resistance, so that the oscillation will be triggered by the thickness and the morphology of the deposit. Whatever the origin of the Hopf-bifurcation, the existence of an oscillation indicates an alternative transition between two antagonistic metastable states having highly different kinetics.

The representation of the same impedance data in a complex capacitance type curve brings some additional information (Fig. 7b). At -1.26 and -1.00V, only a single semicircle assigned to the charging of a double layer is present. This contrasts with the

## a) Chronoamperograms



b) deposit at -0.95 V



c) deposit at -1.20 V

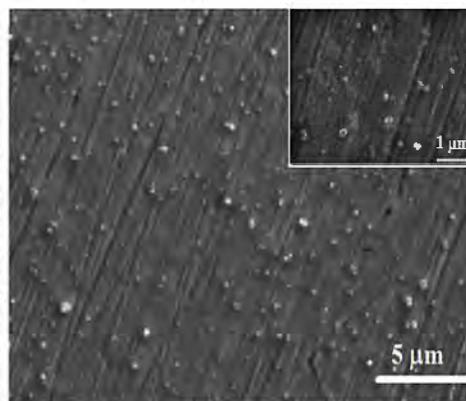


**Fig. 8.** a) Chronoamperograms of deposition processes obtained at 3 different potentials: -0.95 V- black curve, -1.20 V- red curve, -1.40 V- green curve, for 10 minutes. Inset represents first 30 seconds of Chronoamperograms, the brown triangles and blue circles represent fitting curves using Elovich and modified Elovich equations, respectively. 0.12 M Co(TFSI)<sub>2</sub>, T = 100 °C, WE- Pt disc, CE- Pt, RE- Ag/Ag<sub>2</sub>O. b,c - SEM images of deposits obtained at -0.95 V and -1.20 V respectively.

data collected at -1.14 and -1.20 V which present two semicircles, indicative of capacitive phenomena with fast and slow kinetics. Similar results have already been observed in the case of BMPFAPIL, in which the second semicircle was ascribed to charge flow caused by the surface reconstruction (herringbone structures)[33,34].

At this juncture, it is worth mentioning that in pure EMImTFSI IL at 100 °C, the negative impedance and two capacitive semicircles were not observed in the wide potential range of its stability.

### 3.5. Potentiostatic electrodeposition

Having completed the fundamental studies on Co<sup>2+</sup> reduction, we would like now to check the influence of the reported phenomena on the synthesis of Co deposits. Potentiostatic deposition at three different potentials (-0.95; -1.20 and -1.40 V) for 10 min were performed on a Pt disc (Fig. 8a). The morphologies of obtained deposits were checked by SEM (Fig. 8b, c). The j-t curves obtained at -0.95 and -1.40 V almost overlap from the beginning; divergence begins after 125 s, leading to different final current density values of  $j = 2.0 \text{ mA}\cdot\text{cm}^{-2}$  and  $j = 2.6 \text{ mA}\cdot\text{cm}^{-2}$ , respectively. The

curve obtained at -1.20 V shows significantly smaller current density ( $0.95 \text{ mA}\cdot\text{cm}^{-2}$  at the end of the deposition), in agreement with the CV curve, where at this potential a minimum of the current drop was reached. For the deposits taking place at -1.40 and -0.95 V, the j-t data reveal valleys during the first 25 s of deposition (Fig. 8 inset), which we believe to be associated to a 3D nucleation process with diffusion controlled growth[35]. However in the case of the process at -1.20 V, the current decreases drastically from the first seconds. The Elovich equation, commonly used to describe the chemisorption-like phenomena, has been used to fit the first thirty seconds of current profile obtained at -1.20 V (equation 7)[36].

$$-\frac{dQ}{dt} = a \cdot \exp(b \cdot Q) \quad (7)$$

where a, b are fitting parameters and Q is the coverage ratio. Taking into account that  $Q_0 = 0$  at  $t_0 = 0$  and  $Q = Q_n$  at  $t = t_n$  (for  $n > 0$ ), the integrated form of equation 7 is:

$$Q_n = a' + b' \cdot (c + t_n) \quad (8)$$

where a', b' and c are the new fitting parameters. We have assumed that the current is driven by the coverage ratio of an "adsorption

like” phenomenon, so that the concentration of cobalt species in the vicinity of the electrode is constant (the current is not limited by the diffusion phenomenon, which is justified since the deposition current at  $-1.20$  V is much smaller than at  $-0.95$  V). The current equation can be written as:

$$j = -d \frac{dQ}{dt} \quad (9)$$

where  $d$  is the proportionality constant. So the derived equation takes the form:

$$j = \frac{A}{B + t} \quad (10)$$

where  $A$  and  $B$  are the new fitting parameters. The brown triangle curve on the inset (Fig. 8a) represents the fitting with equation 10. A considerable difference between fit and experimental data is observed; the fit curve tends to  $j = 0$  as  $t \rightarrow \infty$ , while the experimental data tends to  $|j| = |j_{\infty}|$  that is higher than 0. The reason for such a difference most likely lies in the fact that the Elovich equation solely describes pure adsorption phenomena. Therefore, we found that a decent fit ( $R^2 = 0.991$ ) could be achieved (Fig. 8a, inset - blue circles) by inserting an additional parameter  $j_{\infty}$  to equation 10, representing the non-zero current also called the leakage current. Thus using equation (11), we could nicely simulate for short deposition times, the experimental results with the parameters as follows:  $A = -1.90$   $\text{mC}\cdot\text{cm}^{-2}$ ,  $B = -2.46$  s and  $j_{\infty} = -0.71$   $\text{mA}\cdot\text{cm}^{-2}$ .

$$j = \frac{A}{B + t} + j_{\infty} \quad (11)$$

Such a correlation suggests that the blocking of the reduction originates from drastic changes in the initial native double layer. For times greater than 30 s, the fitting is no longer valid since an increase in current density is observed, unlike the Elovich equation prediction. This is indicative of the perturbation of the “adsorption” phenomenon by the morphology of the deposited film.

The obtained deposits at  $-0.95$  and  $-1.20$  V were shiny and very adhesive, unlike the one at  $-1.40$  V which detached once the substrate was removed from the solution. In both cases, they consist of a thin layer made of particles ranging from 20 to 100 nm on top of which we could visualize largely dispersed 500 nm to 1  $\mu\text{m}$  size particles (Fig. 8b, c). Lastly, the cracks/scratches observed through our deposits are simply coming from the morphology of the substrate.

#### 4. Discussion

We have reported that the reduction mechanism of  $\text{Co}^{2+}$  in ionic liquid media is rather complex, dependent on many parameters and displaying unusual behavior such as: i) sudden drop in reduction current density at  $-1.2$  V, ii) reduction peak on the oxidation sweep, iii) current profile following the Elovich law, and iv) existence of tricky charge motions as deduced from the negative impedance and the delicate balance between two capacitive semicircles.

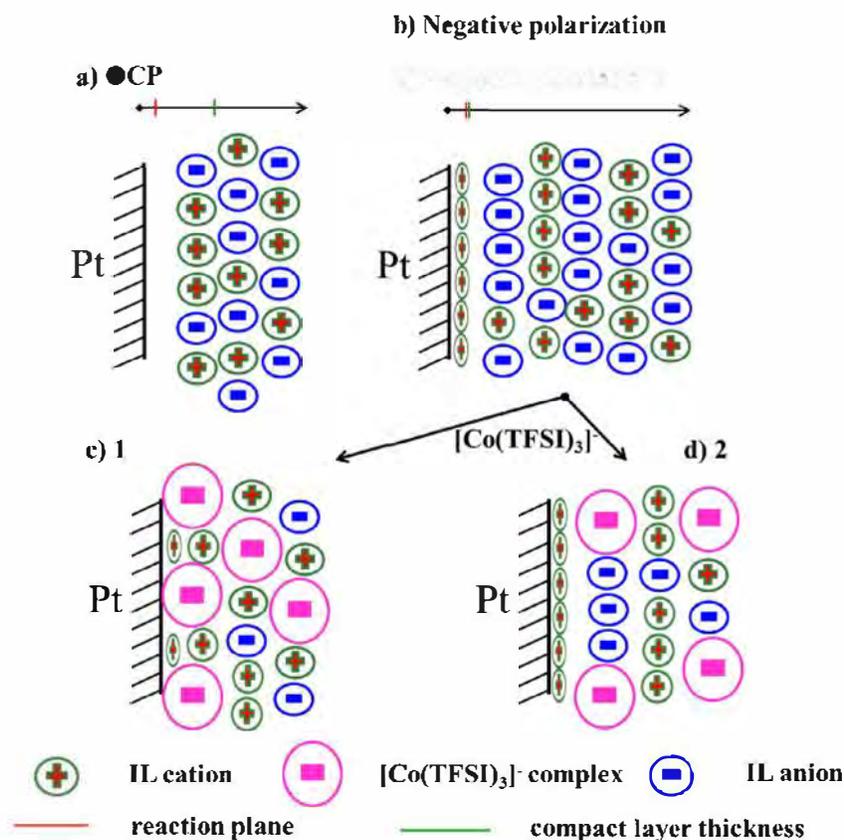
First of all, we should recall that the double layer of pristine ionic liquids in contact with a metal surface is highly structured, especially under additional polarization (Graph 1a, b) where the oscillatory like concentration profiles of cations and anions were observed experimentally and theoretically [13,14,16]. Now, a legitimate question deals with the localization of the cobalt species depending upon concentration, applied potential and so on. We will consider two different scenarios enlisting 1) an uniform distribution of the  $[\text{Co}(\text{TFSI})_3]^-$  complex throughout the double layer, hence disturbing its structure (diffusion of  $[\text{Co}(\text{TFSI})_3]^-$  complex without any obstacle) - Graph 1c, 2) the exclusion of the  $[\text{Co}(\text{TFSI})_3]^-$  complex within the compact layer of the double layer structure (diffusion of  $[\text{Co}(\text{TFSI})_3]^-$  occurs through the compact layer) - Graph 1d. Next, we are trying to decide which of these proposed scenarios is the most likely to be in agreement with our experiments and

existing literature so as to better understand the electrochemical electrodeposition of Co in ionic liquid media, and further try to extend it to other systems.

From the EQCM results, we have a straightforward evidence for an “accumulation” of  $[\text{Co}(\text{TFSI})_3]^-$  complex during the current density drop and further its spontaneous consumption on the reverse sweep (leading to very sharp reduction peak). This is in agreement with our IS spectra that showed the negative impedance in the potential range of sudden current density drop ( $-1.1/-1.2$  V), correlated with the negative slope on the polarization curve. Such behavior is related to the inhibition of the electrochemical process at the electrode as it was already investigated by other groups in aqueous solution [37] and more recently in IL [37,38]. The inhibition may be caused by many different phenomena such as: desorption of electrochemically active species, creation of passive layer, adsorption of surfactant or changes in double layer structuration. Further, the appearance of an oscillating current profile at fixed potential ( $-1.16$  V) suggests an alternative transition between two antagonistic metastable states having highly different kinetics [32,37–39]. Additionally, as investigated by impedance spectroscopy during the current drop phenomenon, a second capacitive semicircle occurred (at low frequencies) that could be assigned to slow surface reconstruction, as for example formation of herringbone structures, although those structures were found only at single crystal oriented electrodes [33,34]. Furthermore, chemisorption-like phenomena are consistent with the current profile of potentiostatic deposition at  $-1.20$  V, which could be well fitted with the modified Elovich equation. All these results suggest that strong interactions between the electrode and the electrolyte occur, which is believed to be linked to the creation of a reversible energetic barrier related to the reconstruction of the double layer upon applied potential.

We also found that the nature of the Ionic Liquid cations as well as the charge of the cobalt complex strongly affect the existence and amplitude of the current density drop. More specifically, the current density drop is very clear when either the cation of IL is based on the ring structure with delocalized electrons (imidazolium based cation) or that the cobalt complex is negatively charged. To the extreme, this drop weakens or even disappears for IL based either on pyrrolidinium or ammonium cations and when positively charged cobalt complex is present. As those two parameters are the major ones influencing on the structure of the double layer, it is becoming doubtful that the scenario 1 (Graph 1c) does occur; indeed the changes in double layer would not affect the state of the  $[\text{Co}(\text{TFSI})_3]^-$  complex. However it would have tremendous impact in scenario 2. With an increase in negative polarization (decrease in potential), the concentration of anions in the first layer of the double layer decreases, because of the electrostatic repulsion. As a consequence, the created cations layer moves towards the electrode surface (thinning of the layer) and finally the double layer gets more structured (e.g. higher number of layers) and compact (Graph 1b). This leads to an increase in both the high potential damping and the viscosity nearby the interface. Those changes can highly affect the electrochemical process taking place at the electrode by disturbing both  $[\text{Co}(\text{TFSI})_3]^-$  diffusion and charge transfer in scenario 2. Additionally, because of its negative charge, the cobalt complex will sit on the second layer (negative charge layer); thus a first cation layer stands as a barrier hindering cobalt from being reduced. Once the charge of the cobalt complex is changed to positive, thanks to the migration flux, it can be directly incorporated in the first layer resulting in the lack of current drop. Overall, taking into account all the above statements, we believe that the energetic barrier at  $-1.20$  V concerns the restructuring of the double layer under applied potential.

Now, it remains to explain why the aforementioned barrier is clearer in imidazolium based ionic liquids. Baldelli et al. [18] found that the imidazolium ring changes the conformation from



**Graph 1.** Draft of the double layer, top part in pure EMImTFSI IL at a) OCP and b) under negative polarization, bottom part—2 possibilities of double layer in EMImTFSI containing  $[\text{Co}(\text{TFSI})_3]^-$  complex under negative polarization c) totally changing the structure of double layer, d) being incorporated in the pristine structure of double layer.

perpendicular to cofacial versus the substrate surface as the negative polarization increases, due to its delocalized positive charge. Consequently, it produces more compact layer (as illustrated on Graph 1b), highly inhibiting the reaction rate. However, this still does not explain the increase in current below  $-1.2\text{ V}$  since according to this theory, the current should drop continuously and not exhibit a minimum as it is visible on the CVs curve. The actual charge transfer reaction plane (place where the electron exchange happens) is not localized at the surface of the electrode but at a distance from it (on the magnitude of few angstroms, Graph 1a, b)[40]. As mentioned above with an increase in negative polarization, the first cation layer becomes thinner and closer to the substrate. Additionally, in case of imidazolium cation based IL metal- $\pi$  interactions can occur so that finally the first cation layer becomes conductive and further reduction of  $[\text{Co}(\text{TFSI})_3]^-$  complex positioned on second layer, can take place. This phenomenon could explain the very low adhesion of the deposit obtained at  $-1.40\text{ V}$ , as a layer of IL cations remains between the substrate and deposit. It would also justify the decrease in oxidation efficiency when the reverse sweep is chosen below the barrier phenomenon (SI, Fig. 1\*). The mechanism of the electron transfer at low and high potentials due to the change in double layer is probably very different; more sophisticated experiments must be performed to probe the validity of this statement. Lastly, it should be noted that in both potential ranges  $-1.0/-1.1\text{ V}$  and  $-1.3/-1.4\text{ V}$ , the reaction limiting parameters are the same since the current values are very similar. On the other hand, if the phenomena are purely caused by surface reconstruction, as in the formation of herringbone structures, the further increase in current would be attributed to the instability of such structures at lower potentials[33].

Another important aspect is the dynamics of this phenomenon. We found that the energetic barrier (minimum of the current drop) shifts to more negative values with an increase in the scanning rate

(SM, Fig. 10\*), suggesting that it is a rather slow phenomenon (in the range of few seconds). Furthermore, the negative loop observed in impedance spectra is visible at frequencies as low as  $0.15\text{ Hz}$ . This is in agreement with previous statements on the origin of the barrier since the changes in the structure of the double layer, which is governed by ion transfer, do not occur rapidly. This can also justify the difference in CV shapes between RT and  $100^\circ\text{C}$  in EMImTFSI IL. At low temperatures, the barrier can actually be enhanced (strong interactions between ions and the substrate), while the reconstructions slowed down (high viscosity/low conductivity); so that only one reduction peak appears at very low potentials during the first scan.

It must be recalled that this is not the only system within which the current suddenly drops leading to a split of the reduction waves or/and the reduction peak on oxidative sweeps. When  $\text{Co}^{2+}$  cations are substituted with  $\text{Mn}^{2+}$ , we experienced the same phenomena, though shifted to more negative potentials (Fig. 9b). With  $\text{Ni}^{2+}$  cations, we solely observe a reduction peak on the reverse sweep (Fig. 9c). Finally, for  $\text{Zn}^{2+}$  cations, neither a drop in current nor the reduction on the reverse sweep (although some small valleys are present) are visible (Fig. 9d). However, the barrier phenomenon for  $\text{Zn}^{2+}$  system was clearly visible in Ionic Liquid containing stronger complexing anions EMImDCA[41], as studied by Forsytech et al. [42]. Baldelli et al. [18] claimed that the BMImdca IL creates a more structured double layer than EMImTFSI (with higher amount of layers that were ascribed to strong coordinating ability of  $\text{DCA}^-$ ); additionally, the viscosity of this IL ( $19.8\text{ cp}$ ) is much smaller than EMImTFSI ( $34\text{ cp}$ ), so that this phenomenon could be observed already at RT. In all cases, the imidazolium cation and negatively charged metal complex are present, therefore there are still other parameters to be considered. Among them, the complex strength may be an important parameter as the  $\text{DCA}^-$  is a much stronger complexing agent than  $\text{TFSI}^-$  (difference in reduction of  $\text{Zn}^{2+}$  in

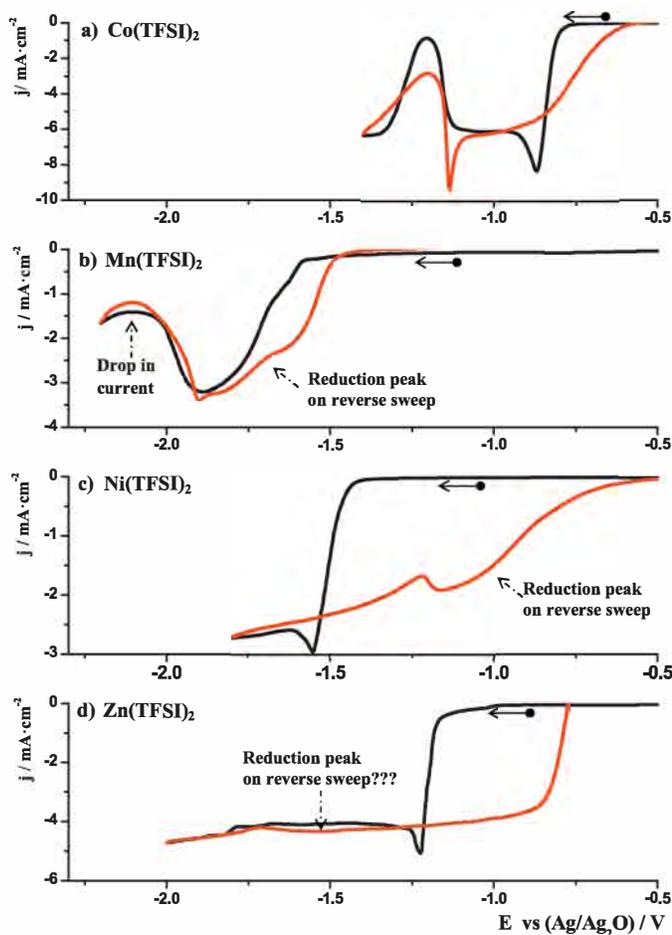


**Fig. 9.** CV curves of EMImTFSI solution at 100 °C containing: a) 0.12 M Co(TFSI)<sub>2</sub>, b) 0.12 M Mn(TFSI)<sub>2</sub>, c) 0.12 M Ni(TFSI)<sub>2</sub>, d) 0.12 M Zn(TFSI)<sub>2</sub>. WE–Ptw, CE–Pt, RE–Ag/Ag<sub>2</sub>O, scanning rate 5 mV·s<sup>-1</sup>.

both IL). The charge density of the complex (the relative charge taking into account the size of the complex) may also be a significant issue. Other systems such as Mn(TFSI)<sub>2</sub> in BMPDCA[41], PdCl<sub>2</sub> in BMImCl[43] and BMPDCA[44], NiCl<sub>2</sub> in BMPDCA[44], or Zn(TfO) in BMPTfO[45] also exhibit uncommon CV curves. Some authors suggest that the two reduction peaks are due to the existence of 2 different metal complexes. This might be true in systems where the metal salt and IL have different anions; it becomes doubtful in our systems where both anions are the same, namely TFSI<sup>-</sup>. Additionally it is not limited to divalent metallic cations since in a solution of TaF<sub>5</sub> in BMPTSI, EMImTFSI and PMImTFSI ILs similar behavior was observed[46].

Although we suspect that the uncommon shape of the CV curve is due to double layer reconstruction, we still do not know what exactly its origin is or how the different metal cation complexes affect it. More detailed experimental work is needed on this topic as well as theoretical modeling, both are ongoing.

## 5. Conclusions

We have reported detailed studies on the reduction of Co<sup>2+</sup> cations in Ionic Liquid media at elevated temperatures, based on the Electrochemical Quartz Crystal Microbalance, Cyclic Voltammetry, Chronoamperometric, Impedance Spectroscopy, Scanning Electron Microscopy and UV-Vis Spectroscopy experiments. An uncommon shape of the CV curve during reduction has been spotted with the sudden current density drop reaching its minimum at -1.2 V and

well defined reduction peak on the reverse sweep. We think this effect to be rooted in the creation of a reversible energetic barrier that prevents from Co<sup>2+</sup> reduction. By a precise adjustment of different bath parameters (substrate, IL formulation, Co<sup>2+</sup> complexation), we found that this phenomenon greatly depends on the nature of the ionic liquid cation and the charge of metal complex although other parameters such as the strength of the cation-anion interaction within the metal complex together with the electronic delocalization should be considered as well. Therefore, we believe that this barrier is nested in the reconstruction of the double layer under applied polarization. Such a phenomenon is not specific to the reduction of Co<sup>2+</sup> in EMImTFSI IL since we show herein that it occurs as well for Mn<sup>2+</sup>, Ni<sup>2+</sup> cations while it has already been reported for Zn<sup>2+</sup>, Pb<sup>2+</sup>, and Pd<sup>2+</sup>.

Finally, the paper shows the importance of tuning precisely the bath solution and specifically the ionic liquid formulation to grow deposits having the desired properties (such as good adhesion) which could find applications within the field of batteries, photovoltaic and microelectronics. We hope this better understanding of the double layer structuring, when working with ionic liquids, will help the community in harvesting all the advantages that ionic liquid media present.

## Acknowledgment

The authors thank P. Simon for fruitful discussions as well as to ALISTORE European Research Institute for the financial support to conduct the research.

## Appendix A. Supplementary data

Supplementary data associated with this article can be found, in the online version, at <https://doi.org/10.1016/j.electacta.2014.03.042>.

## References

- [1] A.A. Aal, R. Al-Salman, M. Al-Zoubi, N. Borissenko, F. Endres, O. Höfft, A. Prowald, S. Zein El Abedin, Interfacial electrochemistry and electrodeposition from some ionic liquids: *In situ* scanning tunneling microscopy, plasma electrochemistry, selenium and macroporous materials, *Electrochimica Acta* 56 (2011) 10295–10305.
- [2] F. Endres, O. Höfft, N. Borisenko, L.H. Gasparotto, A. Prowald, R. Al-Salman, T. Carstens, R. Atkin, A. Bund, S. Zein El Abedin, Do solvation layers of ionic liquids influence electrochemical reactions? *Physical Chemistry Chemical Physics* 12 (2010) 1724–1732.
- [3] F. Endres, S. Zein El Abedin, Air and water stable ionic liquids in physical chemistry, *Physical Chemistry Chemical Physics* 8 (2006), 2101–2016.
- [4] W. Freyland, C.A. Zell, S. Zein El Abedin, F. Endres, Nanoscale electrodeposition of metals and semiconductors from ionic liquids, *Electrochimica Acta* 48 (2003) 3053–3061.
- [5] P. Hapiot, C. Lagrost, *Electrochemical Reactivity in Room-Temperature Ionic Liquids*, *Chemical Reviews* 108 (2008) 2238–2264.
- [6] W. Simka, D. Puszczczyk, G. Nawrat, Electrodeposition of metals from non-aqueous solutions, *Electrochimica Acta* 54 (2009) 5307–5319.
- [7] Y.-Z. Su, Y.-C. Fu, Y.-M. Wei, J.-W. Yan, B.-W. Mao, The Electrode/Ionic Liquid Interface: Electric Double Layer and Metal Electrodeposition, *ChemPhysChem* 11 (2010) 2764–2778.
- [8] Y. Chen, C. Davoisne, J.-M. Tarascon, C. Guéry, Growth of single-crystal copper sulfide thin films via electrodeposition in ionic liquid media for lithium ion batteries, *Journal of Materials Chemistry* 22 (2012) 5295–5299.
- [9] Y. Chen, J.-M. Tarascon, C. Guéry, Exploring sulfur solubility in ionic liquids for the electrodeposition of sulfide films with their electrochemical reactivity toward lithium, *Electrochimica Acta* 99 (2013) 46–53.
- [10] E. Azaceta, R. Marcilla, D. Mecerreyes, M. Ungureanu, A. Dev, T. Voss, S. Fantini, H.-J. Grande, G. Cabanero, R. Tena-Zaera, Electrochemical reduction of O<sub>2</sub> in 1-butyl-1-methylpyrrolidinium bis(trifluoromethanesulfonyl)imide ionic liquid containing Zn<sup>2+</sup> cations: deposition of non-polar oriented ZnO nanocrystalline films, *Physical Chemistry Chemical Physics* 13 (2011) 13433–13440.
- [11] E. Azaceta, S. Chavhan, P. Rossi, M. Paderi, S. Fantini, M. Ungureanu, O. Miguel, H.-J. Grande, R. Tena-Zaera, NiO cathodic electrochemical deposition from an aprotic ionic liquid: Building metal oxide n-p heterojunctions, *Electrochimica Acta* 71 (2012) 39–43.

- [12] M. Tulodziecki, J.M. Tarascon, P.L. Taberna, C. Guéry, Electrodeposition Growth of Oriented ZnO Deposits in Ionic Liquid Media, *Journal of The Electrochemical Society* 159 (2012) D691–D698.
- [13] F. Endres, N. Borisenko, S. Zein El Abedin, R. Hayes, R. Atkin, The interface ionic liquid(s)/electrode(s): *In situ* STM and AFM measurements, *Faraday Discussions* 154 (2012) 221–233.
- [14] C. Merlet, B. Rotenberg, P.A. Madden, P.-L. Taberna, P. Simon, Y. Gogotsi, M. Salanne, On the molecular origin of supercapacitance in nanoporous carbon electrodes, *Nature Materials* 11 (2012) 306–310.
- [15] H. Zhou, M. Rouha, G. Feng, S.S. Lee, H. Docherty, P. Fenter, P.T. Cummings, P.F. Fulvio, S. Dai, J. McDonough, V. Presser, Y. Gogotsi, Nanoscale Perturbations of Room Temperature Ionic Liquid Structure at Charged and Uncharged Interfaces, *ACS Nano* 6 (2012) 9818–9827.
- [16] S. Baldelli, Interfacial Structure of Room-Temperature Ionic Liquids at the Solid-Liquid Interface as Probed by Sum Frequency Generation Spectroscopy, *The Journal of Physical Chemistry Letters* 4 (2013) 244–252.
- [17] T. Carstens, R. Hayes, S. Zein El Abedin, B. Corr, G.B. Webber, N. Borisenko, R. Atkin, F. Endres, *In situ* STM, AFM and DTS study of the interface 1-hexyl-3-methylimidazolium tris(pentafluoroethyl)trifluorophosphate/Au(111), *Electrochimica Acta* 82 (2012) 48–59.
- [18] S. Baldelli, Surface Structure at the Ionic Liquid-Electrified Metal Interface, *Accounts of Chemical Research* 41 (2008) 421–431.
- [19] N. Pradhan, T. Subbaiah, S.C. Das, Effect of Zinc on the Electrocrystallization of Cobalt, *Journal of Applied Electrochemistry* 27 (1997) 713–719.
- [20] S.P. Jiang, A.C.C. Tseung, Reactive Deposition of Cobalt Electrodes, *Journal of Electrochemical Society* 137 (1990) 3387–3393.
- [21] Y. Katayama, R. Fukui, T. Miura, Electrodeposition of Cobalt from an Imide-Type Room-Temperature Ionic Liquid, *Journal of The Electrochemical Society* 154 (2007) D534–D537.
- [22] R. Fukui, Y. Katayama, T. Miura, The effect of organic additives in electrodeposition of Co from an amide-type ionic liquid, *Electrochimica Acta* 56 (2011) 1190–1196.
- [23] C. Su, M. An, P. Yang, H. Gu, X. Guo, Electrochemical behavior of cobalt from 1-butyl-3-methylimidazolium tetrafluoroborate ionic liquid, *Applied Surface Science* 256 (2010) 4888–4893.
- [24] S. Schaltin, P. Nockemann, B. Thijs, K. Binnemans, J. Fransaer, Influence of the anion on the electrodeposition of cobalt from imidazolium ionic liquids, *Electrochemical and Solid-State Letters* 10 (2007) D104–D107.
- [25] M.A. Saito, J.W. Moffett, Complexation of cobalt by natural organic ligands in the Sargasso Sea as determined by a new high-sensitivity electrochemical cobalt speciation method suitable for open ocean work, *Marine Chemistry* 75 (2001) 49–68.
- [26] K. Fujii, T. Nonaka, Y. Akimoto, Y. Umabayashi, S.-i. Ishiguro, Solvation Structures of Some Transition Metal(II) Ions in a Room-Temperature Ionic Liquid, 1-Ethyl-3-methylimidazolium Bis(trifluoromethanesulfonyl)amide, *Analytical Sciences* 24 (2008) 1377–1380.
- [27] Y. Sugawara, T. Okayasu, A.P. Yadav, A. Nishikata, T. Tsuru, Dissolution Mechanism of Platinum in Sulfuric Acid Solution, *Journal of The Electrochemical Society* 159 (2012) F779–F786.
- [28] S. Bruckenstein, M. Shay, Experimental Aspects of Use of the Quartz Crystal Microbalance in Solution, *Electrochimica Acta* 30 (1985) 1295–1300.
- [29] L.-S. Liu, J. Kim, S.-M. Chang, G.J. Choi, W.-S. Kim, Quartz Crystal Microbalance Technique for Analysis of Cooling Crystallization, *Analytical Chemistry* 85 (2013) 4790–4796.
- [30] G. Sauerbrey, Verwendung von Schwingquarzen zur Wagung Dunner Schichten und zur Mikrowagung, *Zeitschrift für Physik* 155 (1959) 206–222.
- [31] A. Bund, O. Schneider, V. Dehnke, Combining AFM and EQCM for the *in situ* investigation of surface roughness effects during electrochemical metal depositions, *Physical Chemistry Chemical Physics* 4 (2002) 3552–3554.
- [32] M.T.M. Koper, Non-linear phenomena in electrochemical systems, *Journal of The Chemical Society, Faraday Transactions* 94 (1998) 1369–1378.
- [33] R. Atkin, N. Borisenko, M. Drüscler, S. Zein El Abedin, F. Endres, R. Hayes, B. Huber, B. Røling, An *in situ* STM/AFM and impedance spectroscopy study of the extremely pure 1-butyl-1-methylpyrrolidinium tris(pentafluoroethyl)trifluorophosphate/Au(111) interface: potential dependent solvation layers and the herringbone reconstruction, *Physical Chemistry Chemical Physics* 13 (2011) 6849–6857.
- [34] M. Drüscler, N. Borisenko, J. Wallauer, C. Winter, B. Huber, F. Endres, B. Røling, New insights into the interface between a single-crystalline metal electrode and an extremely pure ionic liquid: slow interfacial processes and the influence of temperature on interfacial dynamics, *Physical Chemistry Chemical Physics* 14 (2012) 5090–5099.
- [35] E.L. Smith, J.C. Barron, A.P. Abbott, K.S. Ryder, Time Resolved *In Situ* Liquid Atomic Force Microscopy and Simultaneous Acoustic Impedance Electrochemical Quartz Crystal Microbalance Measurements: A Study of Zn Deposition, *Analytical Chemistry* 81 (2009) 8466–8471.
- [36] F.-C. Wu, R.-L. Tseng, R.-S. Juang, Characteristics of Elovich equation used for the analysis of adsorption kinetics in dye-chitosan systems, *Chemical Engineering Journal* 150 (2009) 366–373.
- [37] I.Z. Kiss, V. Gáspár, Stability Analysis of the Oscillatory Electrodeposition of Copper with Impedance Spectroscopy, *The Journal of Physical Chemistry A* 102 (1998) 909–914.
- [38] S. Schaltin, K. Binnemans, J. Fransaer, Oscillating electrochemical reaction in copper-containing imidazolium ionic liquids, *Physical Chemistry Chemical Physics* 13 (2011) 15448–15454.
- [39] A. Survila, Z. Mockus, R. Juškenas, Current oscillations observed during codeposition of copper and tin from sulfate solution, *Electrochimica Acta* 43 (1998) 909–917.
- [40] A.A. Franco, P. Schott, C. Jallut, B. Maschke, A Dynamic Mechanistic Model of an Electrochemical Interface, *Journal of The Electrochemical Society* 153 (2006) A1053–A1061.
- [41] M.-J. Deng, P.-Y. Chen, T.-I. Leong, I.-W. Sun, J.-K. Chang, W.-T. Tsai, Dicyanamide anion based ionic liquids for electrodeposition of metals, *Electrochemistry Communications* 10 (2008) 213–216.
- [42] T.J. Simons, A.A.J. Torriero, P.C. Howlett, D.R. MacFarlane, M. Forsyth, High current density, efficient cycling of Zn<sup>2+</sup> in 1-ethyl-3-methylimidazolium dicyanamide ionic liquid: The effect of Zn<sup>2+</sup> salt and water concentration, *Electrochemistry Communications* 18 (2012) 119–122.
- [43] M. Jayakumar, K.A. Venkatesan, T.G. Srinivasan, P.R. Vasudeva Rao, Electrochemical behavior of ruthenium (III), rhodium (III) and palladium (II) in 1-butyl-3-methylimidazolium chloride ionic liquid, *Electrochimica Acta* 54 (2009) 6747–6755.
- [44] H.-Y. Huang, P.-Y. Chen, Voltammetric behavior of Pd(II) and Ni(II) ions and electrodeposition of PdNi bimetal in *N*-butyl-*N*-methylpyrrolidinium dicyanamide ionic liquid, *Electrochimica Acta* 56 (2011) 2336–2343.
- [45] Z. Liu, A. Prowald, S. Zein El Abedin, F. Endres, Template-assisted electrodeposition of highly ordered macroporous zinc structures from an ionic liquid, *Journal of Solid State Electrochemistry* 17 (2013) 1185–1188.
- [46] A. Ispas, B. Adolph, A. Bund, F. Endres, On the electrodeposition of tantalum from three different ionic liquids with the bis(trifluoromethyl sulfonyl) amide anion, *Physical Chemistry Chemical Physics* 12 (2010) 1793–1803.